Hindawi Publishing Corporation
Journal of Nanomaterials
Volume 2015, Article ID 680306, 9 pages
http://dx.doi.org/10.1155/2015/680306

Research Article

Controlled Synthesis of Hierarchically Assembled Porous ZnO Microspheres with Enhanced Gas-Sensing Properties

Shengsheng You,[1] Haojie Song,[1] Jing Qian,[1] Ya-li Sun,[1] and Xiao-hua Jia[2]

[1]*Institute of Polymer Materials, School of Materials Science & Engineering, Jiangsu University, Zhenjiang 212013, China*
[2]*School of Environment and Safety Engineering, Jiangsu University, Zhenjiang, Jiangsu 212013, China*

Correspondence should be addressed to Xiao-hua Jia; xhjia2003@126.com

Received 7 April 2015; Revised 13 July 2015; Accepted 16 July 2015

Academic Editor: Nguyen V. Hieu

The ZnO microspheres constructed by porous nanosheets were successfully synthesized by calcinating zinc hydroxide carbonate (ZHC) microspheres obtained by a sample hydrothermal method. The samples were characterized in detail with scanning electron microscopy (SEM), transmission electron microscopy (TEM), X-ray diffraction (XRD), and thermogravimetric and differential scanning calorimetry (TG-DSC). The results indicated that the prepared ZnO microspheres were well crystalline with wurtzite hexagonal phase. The effects of reaction time, temperature, the amount of trisodium citrate, and urea on the morphology of ZnO microspheres were studied. The formation mechanism of porous ZnO microspheres was discussed. Furthermore, the gas-sensing properties for detection of organic gas of the prepared porous ZnO microspheres were investigated. The results indicated that the prepared porous ZnO microspheres exhibited high gas-sensing properties for detection of ethanol gas.

1. Introduction

Zinc oxide (ZnO) is one of the most important n-type semiconductor materials with a direct wide band gap (3.37 eV) and large excitation binding energy (60 meV) [1]. It has attracted great attention for a long time due to its luminous, piezoelectric, electroconductive, gas-sensing, and photocatalytic [2–6] properties that has broad applications in the field such as lighting emitting diode, ultraviolet detectors, gas sensors, varistors, solar cells, and photocatalysts [7–12]. In addition, ZnO has abundant raw materials, cheap price, no toxicity, and simple synthetic method [13], and therefore ZnO has been recognized as one of the most important promising semiconductor materials. More and more research groups have been concentrated on using ZnO as a gas sensor for a variety of gases such as NH_3, formaldehyde, CO, H_2S, ethanol, and NO_2 [14–19]. In recent years, many researchers have devoted themselves to synthesis of ZnO with different morphologies for special applications. To date, ZnO with various size and morphologies have been reported, such as one-dimensional ZnO nanostructures, including nanotubes, nanorods, and nanowires, and two-dimensional (2D) ZnO nanosheets, nanofilm [20–24]. However, compared with those ZnO materials above, 3D ZnO structures exhibited superior gas-sensing properties [25], which may be attributed to their high specific surface area, good permeability, and high interfacial charge-transfer efficiency [26].

It is known that the morphology, microstructures, and gas-sensing activity of ZnO are significantly influenced by the preparative conditions and methods. Numerous chemical and physicochemical methods have been developed to synthesize the 3D ZnO nanostructures. For example, Gu et al. [27] synthesized 3D flower-like ZnO nanostructures by microwave-assisted method. Li et al. [28] fabricated ZnO 3D microstructures with nano-multipod by thermal evaporation methods using metal catalysts. Cai et al. [29] reported that awl-like ZnO nanostructures have been fabricated by sublimation process employing chemical vapor deposition (CVD) method. However, these synthesis methods typically involve complex controlling process and too much energy, which possibly result in the increased cost and limitation of the potential applications. Therefore, the development of a facile, effective, and economical approach to synthesize ZnO and control of their morphology are strongly desirable. The most promising one was thermal decomposition or calcination of zinc carbonate and zinc carbonate hydroxide precursors.

The raw materials for this process are easily available and have a low-cost, superfine ZnO product which can be easily prepared by using this technique [30].

In this work, the porous ZnO microspheres constructed by multilayered porous nanosheets were obtained through a hydrothermal preparation and a thermal decomposition. The synthesized porous ZnO microspheres are assembled by numerous porous nanosheets. We investigated the effect of ZnO microsphere synthesis parameters. On the basis of the experimental results and analysis, the formation mechanism of the porous ZnO microspheres was pointed out. The prepared samples exhibited excellent sensing performance to ethanol gas, and the porous ZnO microspheres were promising candidates for the applications of ethanol sensitive material.

2. Experimental Section

2.1. Synthesis of ZnO Porous Microspheres. All chemicals used were of analytical grade from Shanghai Chemical Reagent Corporation and without further purification. ZnO porous microspheres constructed by multilayered porous nanosheets have been fabricated via hydrothermal method and a thermal decomposition. In a typical synthesis process, 3 mmol zinc nitrate hexahydrate ($Zn(NO_3)_2{\cdot}6H_2O$), 6 mmol urea ($CO(NH_2)_2$), and 0.5 mmol trisodium citrate were dissolved in 100 mL deionized water by a magnetic stirrer to form a mixed solution; the mixed solution was transferred into a 100 mL teflon-lined stainless steel autoclave and heated at 120°C for 6 h. The precipitate was collected by centrifugation and washed thoroughly with deionized water several times to remove the impurities and dried in a vacuum oven at 60°C for 12 h to obtain the ZHC precursors.

For the synthesis of porous ZnO microspheres, the as-obtained precursors were placed in a crucible and heated from room temperature to 500°C at a rate of 10°C/min and then maintained at 500°C for 2 h in air. After cooling to room temperature, the final product was collected.

2.2. Characterization. The phase structure and compositions of the as-fabricated products were identified by X-ray diffraction (XRD, Philips X'pert X-ray diffractometer with Cu-Kα radiation, λ = 1.5406 Å) at 40 kV, 30 mA over the 2θ range 10–80°. Thermogravimetric (TG) and differential scanning calorimetry (DSC) analysis was measured by a thermogravimetric analyzer (NETZSCH STA 409 PC) with a heating temperature rate of 5°C min^{-1} under atmosphere from 50°C to 1000°C. The morphology and microstructure of the products were further investigated by scanning electron microscopy (SEM) using a JEOL JSM 6700F and transmission electron microscopy (TEM) using a JEOL JEM 2010F microscope working at 200 kV. The Brunauer-Emmett-Teller (BET) surface areas of the products were analyzed using a Micromeritics ASAP 2020 nitrogen adsorption apparatus.

2.3. Gas-Sensing Properties Test. For gas sensor experiments, the ZnO product was mixed with deionized water to form a paste and then coated onto an alumina tube-like substrate, on which a pair of platinum wires had been installed. The ZnO coated substrate was dried under IR radiation in the air and then annealed at 500°C in air for 2 h. At last, a small Ni–Cr alloy coil was placed penetrating into the tube as a heater. The gas sensor was aged at 450°C in air for 10 days in order to improve the long-term stability and repeatability.

The gas-sensing properties of ZnO porous microspheres were tested using a WS-30A gas sensitivity system (Winsen Instruments Co., Zhengzhou, China). A certain concentration of target gas was injected into the evaporator in the sealed glass chamber separately and then mixed by starting the pair of air small-sized fans. The gas response value of testing gas was defined as the ratio of R_a to R_g, where R_a and R_g represent the resistance of the as-obtained ZnO measured in air and testing gas environment, respectively.

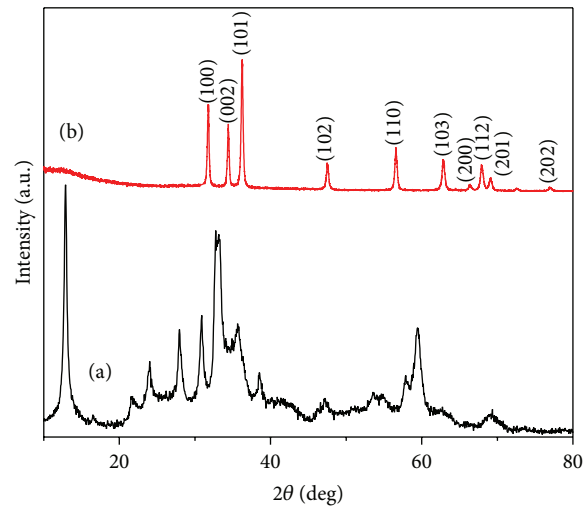

Figure 1: XRD pattern of (a) the ZnHC precursors and (b) ZnO obtained after being annealed at 500°C for 2 h.

3. Results and Discussion

Figure 1 shows the XRD pattern of the ZHC precursors (Figure 1(a)). All the diffraction peaks in Figure 1(a) can be indexed as monoclinic zinc hydroxide carbonate $Zn_5(OH)_6(CO_3)_2$ (JCPDS Card Number 11-0287). As shown in Figure 1(b), the diffraction peaks of ZnO porous microspheres correspond well with the (100), (002), (101), (102), (110), (103), (200), (112), (201), and (202) reflections of the hexagonal wurtzite structure of ZnO (space group P63mc, JCPDS Card Number 36-1451, a = 3.25 Å, c = 5.207 Å). No characteristic peaks of other impurities were detected in the XRD patterns, indicating that the porous ZnO microspheres had high purity and good crystallinity. That is to say, the ZHC precursors can be transformed utterly to a pure phase of hexagonal wurtzite type ZnO after being annealed at 500°C for 2 h.

The morphology and microstructure of the ZHC precursors and the ZnO microspheres were examined by SEM (Figure 2). Figure 2(a) shows the SEM image of an individual

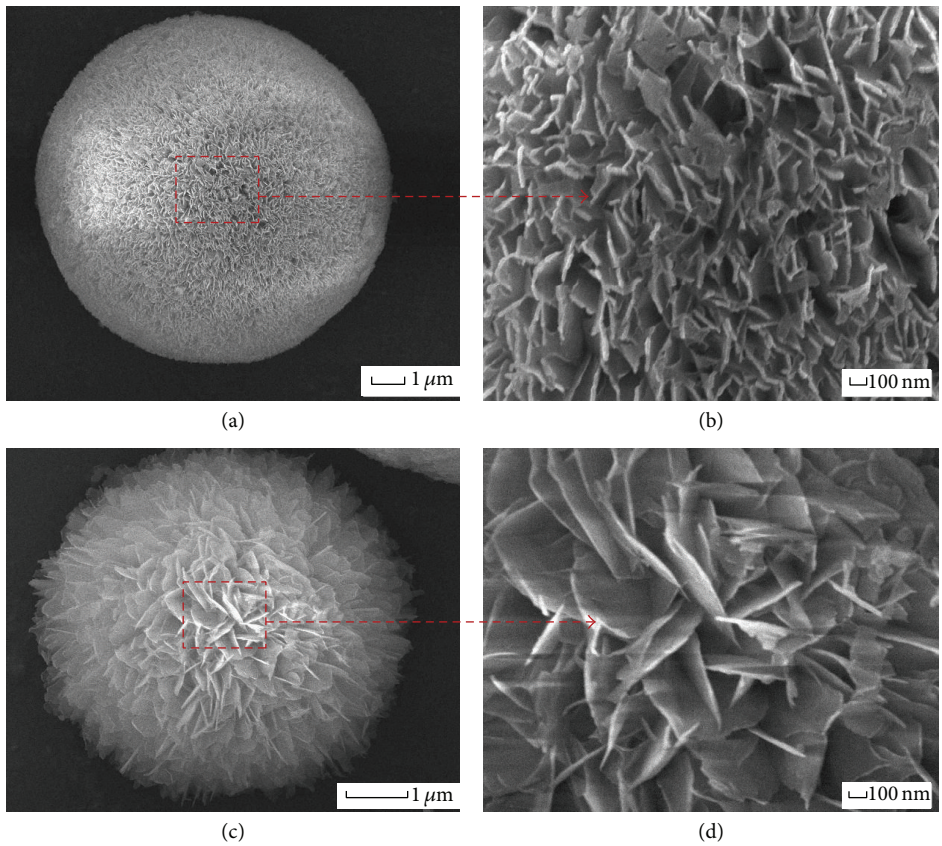

Figure 2: ((a) and (b)) SEM images of the ZHC precursors; ((c) and (d)) SEM images of ZnO porous microspheres obtained at 500°C for 2 h.

ZHC precursors microsphere. It demonstrates that the microsphere was assembled by many nanosheets, which are intercrossed with each other (Figure 2(b)). Figures 2(c) and 2(d) show the SEM images of ZnO microspheres, which calcined at 500°C in air for 2 h. Compared to the samples before calcination, the morphology and size of the calcined samples had no obvious change. It reveals that high-temperature calcining process did not destroy the 3D hierarchical structure, while the assembled structure becomes a little loose and the surface was rougher than uncalcined samples.

The porous ZnO nanosheets are further characterized by the TEM. Compared to the TEM images of ZHC precursors (Figure 3(a)), it can be seen that many pores of various sizes were observed on the surfaces of the nanosheets from the TEM images (Figures 3(b) and 3(c)) of ZnO nanosheets, due to the fact that the ZHC precursors were decomposed under the high temperature and then the water and carbon dioxide were volatilized. The porous ZnO microspheres, synthesized by hydrothermal method and a thermal decomposition, have large specific surface area and many active centers [31]. To obtain further information about the specific surface area and the pore sizes distribution of the as-prepared ZnO microspheres, nitrogen adsorption-desorption analysis was performed. As shown in Figure 3(d), the nitrogen adsorption-desorption isotherm belongs to type IV, indicating the existence of abundant mesopores in the ZnO microspheres. Using the BJH method and the desorption branch of the nitrogen isotherm, the calculated pore-size distribution indicates that the material contains an average pore size of 25.288 nm. The specific surface area of the ZnO microspheres is calculated to be 29.87 m^2/g by the BET equation. As-synthesized ZnO microspheres with a high special surface area may provide more surface active sites and pore-channels for gas sensing.

TG-DSC curves of the ZHC precursors were shown in Figure 4. It is obvious that TG curve of ZHC precursors contains two distinct weight loss steps. The weight loss in 50–200°C is 5.6 wt%, due to the endothermic loss of surface hydroxyls and water molecules in the precursors. The maximum weight loss occurring in the second step between 200 and 500°C is 22.1 wt% due to the volatilization of carbon dioxide. There is a strong endothermic peak at 257°C in the DSC curve, which corresponds with the second weight loss. There is no obvious weight loss on TG curve after 500°C, indicating the ZHC precursors were completely decomposed.

The SEM images of the ZnO samples at different reaction temperatures (120°C and 150°C) were shown in Figures 5(a) and 5(b). At 120°C, the samples had a spherical structure with diameter of about 3 μm (Figure 5(a)). When the reaction temperature increased to 150°C (Figure 5(b)), the samples had a spherical structure with diameter of approximately 6 μm. As raising the reaction temperature, the size of the ZnO microspheres increased. It was demonstrated that the decomposition rate of urea will be increased with increasing

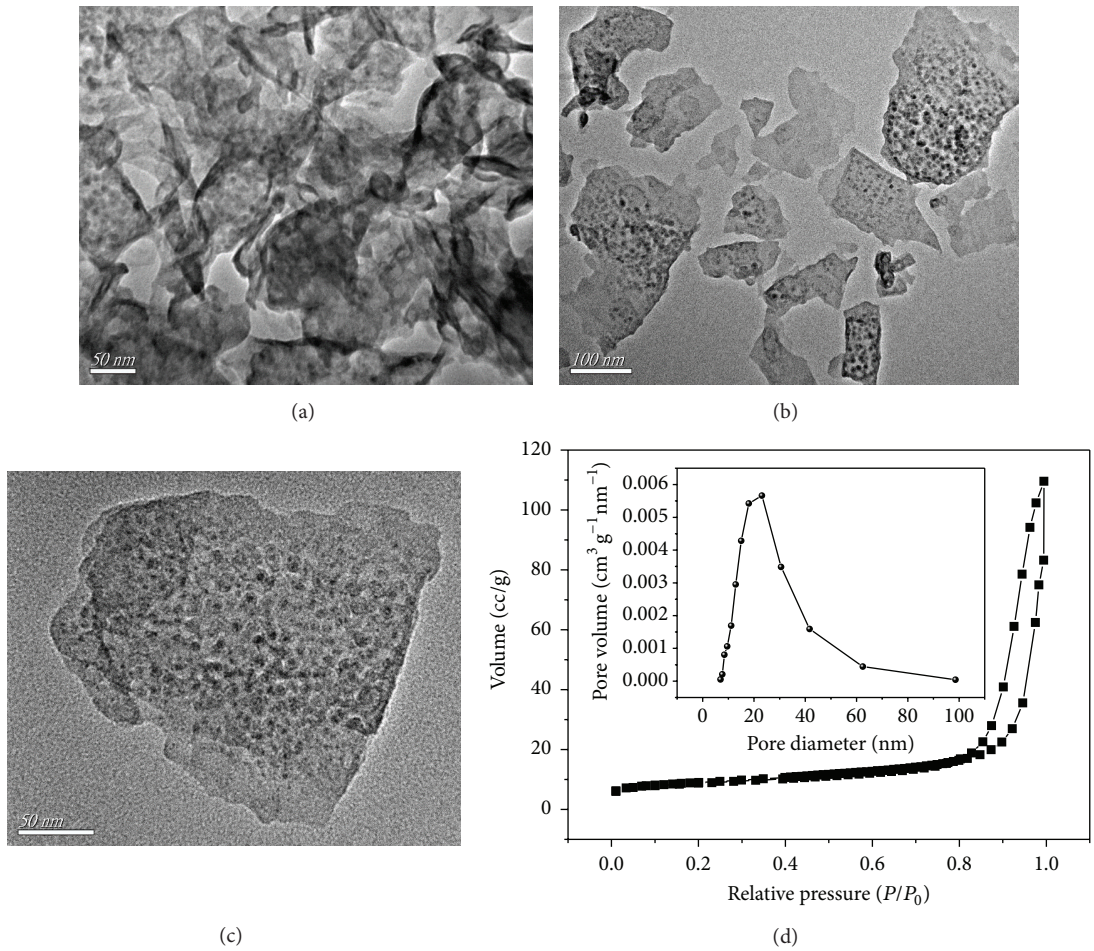

Figure 3: (a) TEM images of the ZHC precursors nanosheets; ((b) and (c)) TEM images of porous ZnO nanosheets; (d) N_2 adsorption-desorption isotherm and BJH pore size distribution plots (inset) of the porous ZnO product calcined ZHC precursors.

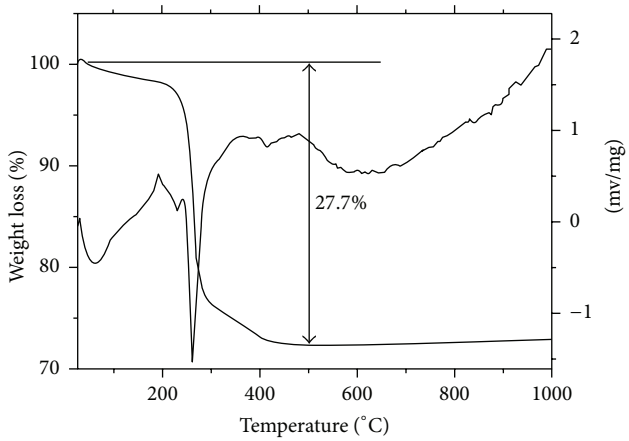

Figure 4: TG and DSC curves of the ZHC precursors.

reaction temperature. The amount of precipitation agent also increases in unit time promoting the nucleation and growth of grain. In order to understand the effects of reaction time on the sample structure, time-dependent experiments were carried out at 120°C. Figures 5(c) and 5(d) show the SEM images of the samples synthesized at 120°C for different reaction time. As shown in Figure 5(c), the size of the ZnO microspheres is not homogeneous. While the reaction time is up to 3 h, it can be seen from Figure 5(d) that the ZnO microspheres are more regular and the size of sample is becoming more uniform. Thus, the ZnO microspheres tend to be uniform and regular when prolonging the reaction time.

The amount of trisodium citrate has an important influence on the sample structure. Different amounts of trisodium citrate (0, 0.5 mmol) were carried out in the experiments. The SEM images of the ZnO microspheres in the different conditions were shown in Figures 6(a) and 6(b). From Figure 6(a), it can be seen that the nanosheets aggregate irregularly and the size is bigger without trisodium citrate in the reaction. With increasing of trisodium citrate, the nanosheets become shorter and self-assemble into a spherical structure. It was demonstrated that trisodium citrate can inhibit the further growth of nanosheets and promote nanosheets assembly into a spherical structure.

Urea, as precipitant, plays an important role in the whole reaction. The SEM images of the ZnO microspheres were prepared by different amount of urea which were shown in

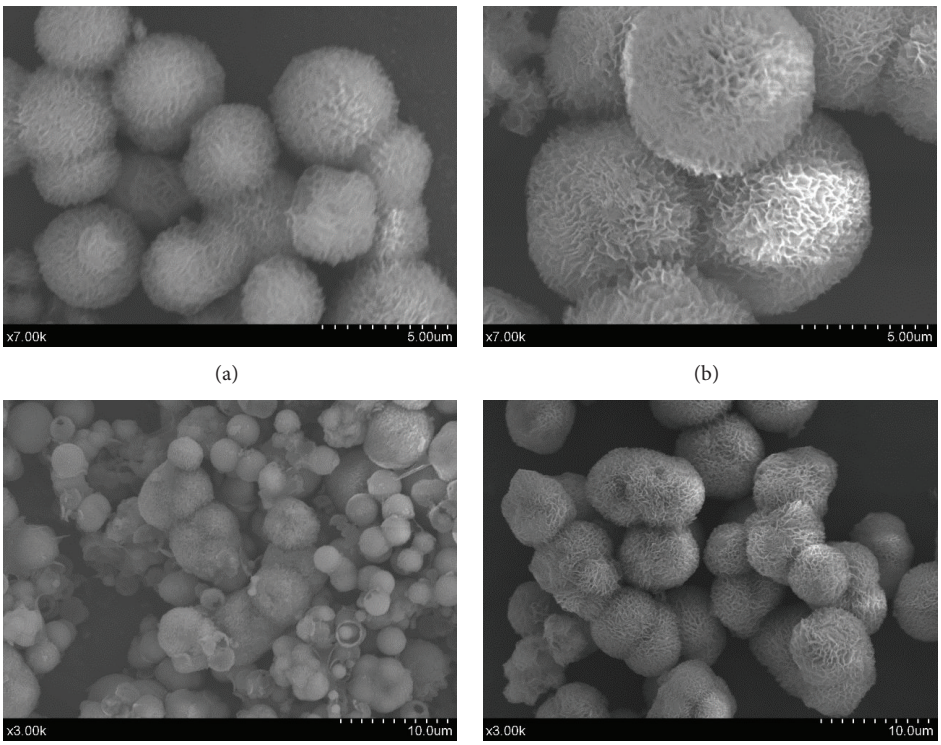

Figure 5: SEM images of the samples synthesized at different reaction times and temperatures: (a) 120°C; (b) 150°C; (c) 1 h; (d) 3 h.

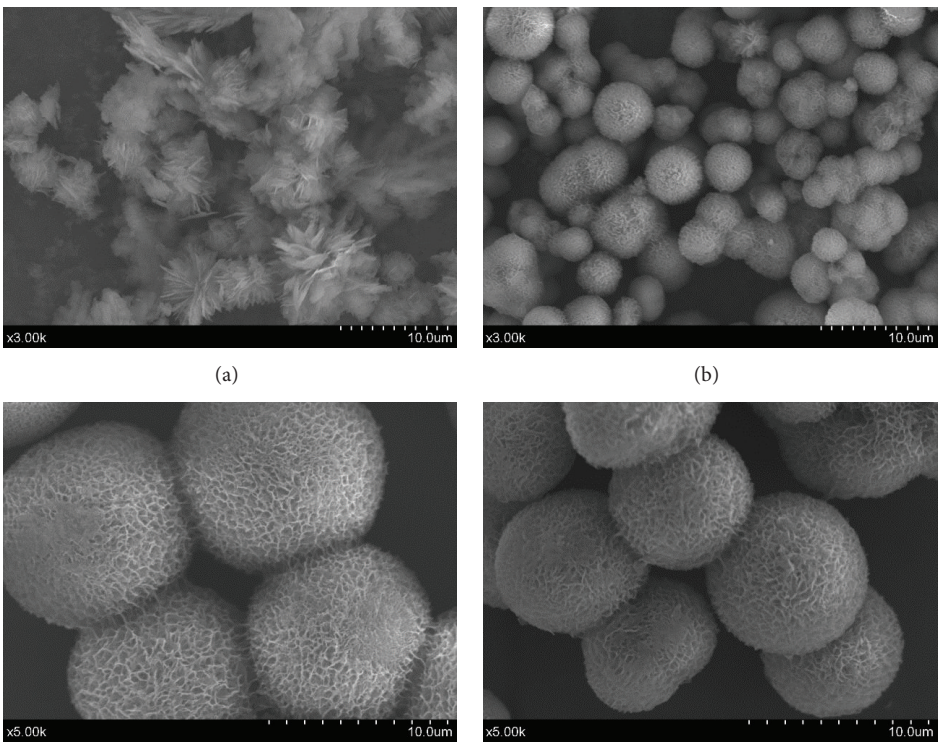

Figure 6: SEM images of the as-prepared ZnO microspheres synthesized under the different amount of trisodium citrate and urea: (a) 0 mmol trisodium citrate; (b) 0.5 mmol trisodium citrate; (c) 3 mmol urea; (d) 4 mmol urea.

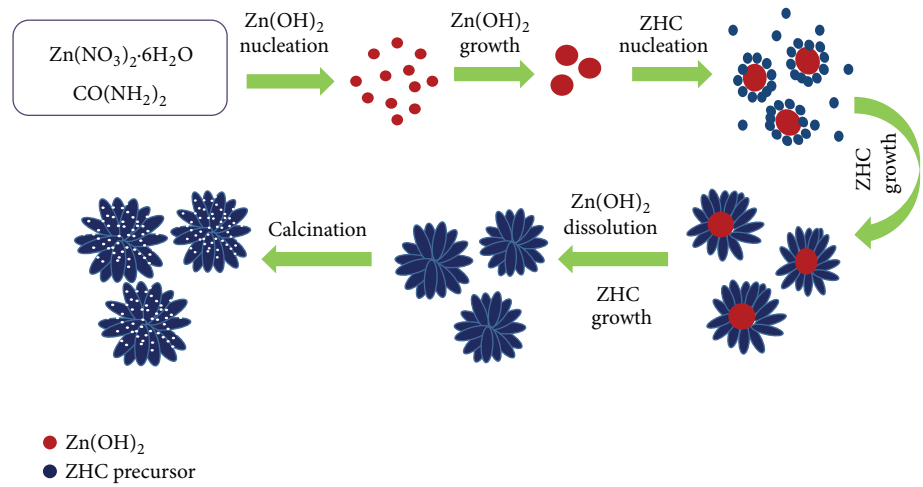

Figure 7: Schematic illustrations of growth mechanism of the porous ZnO microspheres.

Figures 6(c) and 6(d). When the amount of urea is 3 mmol, the samples had a spherical structure and relatively uniform sizes with diameter of about 8 μm. When the amount of urea increased to 4 mmol (Figure 6(d)), the samples had a spherical structure with diameter of approximately 6 μm. Compared with Figure 6(d), the size of the microspheres shown in Figure 6(c) becomes smaller, owing to the increasing of urea, and the reaction points of ZnO microspheres become more. Based on the above analysis, it can be seen that the amount of urea can affect the size of ZnO microspheres.

Based on the above experimental results and analysis, we proposed the growth mechanism of the porous ZnO microspheres. The formation mechanism was shown in Figure 7. In this formation process, trisodium citrate and urea were used as complexant and precipitant, respectively. The chemical reactions can be written as follows:

$$(NH_2)_2\,CO + 3H_2O \longrightarrow 2NH_3 \cdot H_2O + CO_2 \quad (1)$$

$$NH_3 \cdot H_2O \longrightarrow NH^{4+} + OH^- \quad (2)$$

$$CO_2 + 2OH^- \longrightarrow {CO_3}^{2-} + H_2O \quad (3)$$

$$Zn^{2+} + 2OH^- \longrightarrow Zn\,(OH)_2 \quad (4)$$

$$5Zn^{2+} + 6OH^- + 2{CO_3}^{2-} \longrightarrow Zn_5\,(OH)_6\,(CO_3)_2 \quad (5)$$

$$5Zn\,(OH)_2 + 2{CO_3}^{2-} \longrightarrow Zn_5\,(OH)_6\,(CO_3)_2 + 4OH^- \quad (6)$$

$$Zn_5\,(OH)_6\,(CO_3)_2 \longrightarrow 5ZnO + 3H_2O + 2CO_2 \quad (7)$$

At the beginning of reaction, the solution is neutral. when the temperature exceeds 80°C, the urea begins to decompose, and then OH^- obtained from the reactions (1) and (2) will react with Zn^{2+} and generate $Zn(OH)_2$ (reaction (4)). As the reaction proceeded, solution becomes saturated gradually, $Zn(OH)_2$ starts to nucleate and then grows further into $Zn(OH)_2$ spheres. According to the reaction (3), the concentration of ${CO_3}^{2-}$ in solution is increasing with the reaction proceeding, and then Zn^{2+} and OH^- react with ${CO_3}^{2-}$ (reaction (5)) and generate ZHC precursor on the surface of $Zn(OH)_2$ spheres. As the reaction progresses, the concentration of Zn^{2+} in the solution decreased, in order to supplement the Zn^{2+}, the $Zn(OH)_2$ spheres begin to dissolve gradually, and then more and more nanosheets grow out from a crystal nucleus (reaction (6)) and finally assemble into the ZHC precursor spheres. The $Zn(OH)_2$ spheres disappeared and ZHC precursor microspheres formed completely after 6 h.

In the process of the reaction, trisodium citrate as complexing agent has very important influence on the morphology of the samples. Citrate anion ($C_5H_7O_5COO^-$) and Zn^{2+} formed complex, hindering the reaction of Zn^{2+}, OH^-, and ${CO_3}^{2-}$, which slows down the formation velocity of ZHC precursor and controls the morphology of precursors. In addition, the citrate ions can be adsorbed on the surface of nanosheets effectively, limiting the horizontal and vertical growth of the nanosheets. Finally, the ZHC precursors were calcinated at 500°C for 2 h in the air condition, the porous ZnO microspheres were obtained, owing to the ZHC precursors decomposed in the calcination process, and then the water and carbon dioxide were volatilized (reaction (7)).

In the end, we tested the gas-sensing performances of the sensors based on the flower-like porous ZnO microspheres, which were synthesized by a simple hydrothermal method with zinc nitrate hexahydrate (3 mmol), urea (6 mmol), and trisodium citrate (0.5 mmol) as raw materials at 120°C for 6 h. In order to determine the optimal operating temperature, gas response of the sensors based on porous ZnO microspheres toward 50 ppm ethanol was investigated at different operating temperature, and the result is shown in Figure 8(a). It can be seen that the response to ethanol gas increased rapidly with the increase in operating temperature from 220 to 280°C and reached maximum at 280°C. After that, the response decreased with further increase in the operating temperature. Obviously, the optimal operating temperature

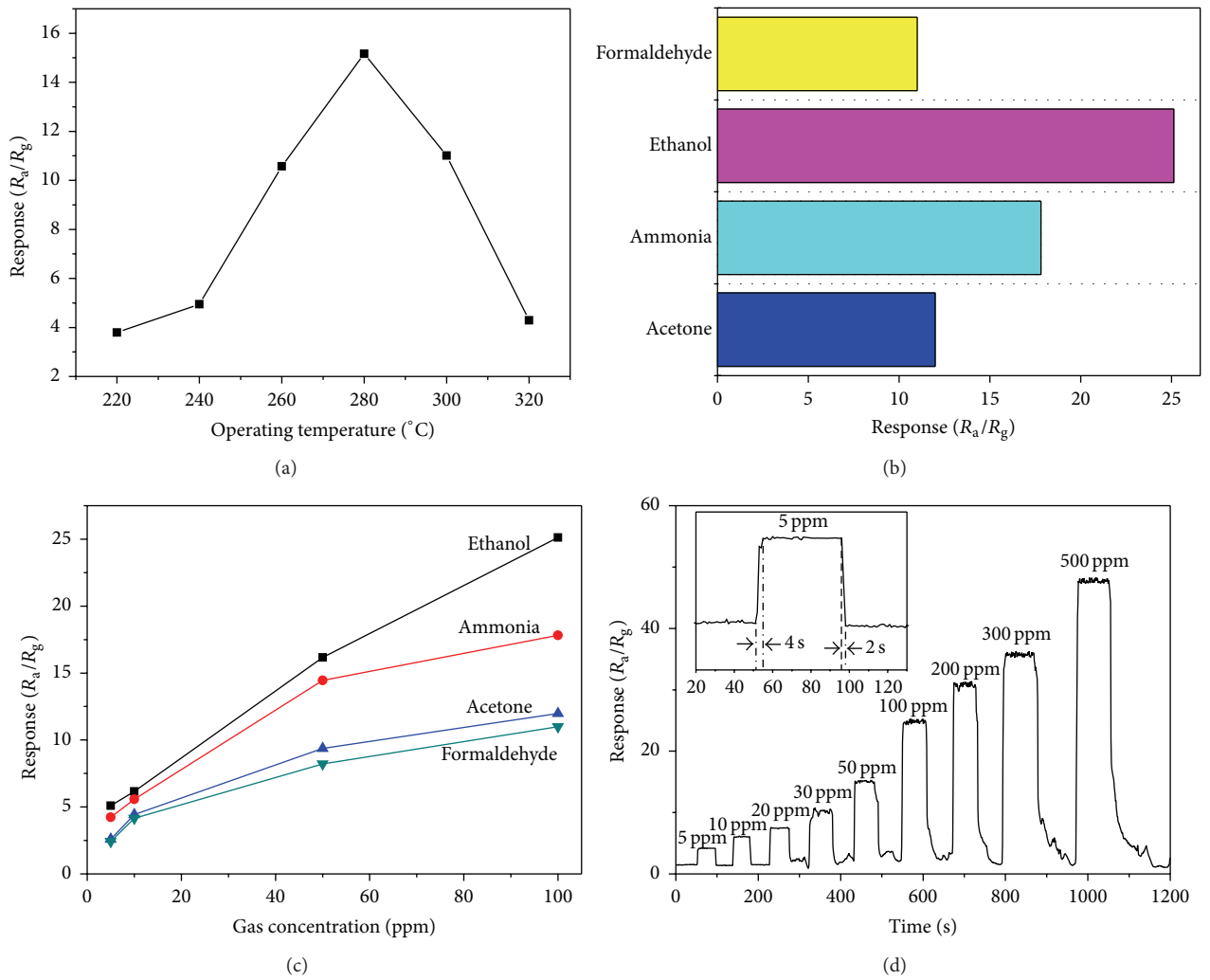

FIGURE 8: (a) Effect of operating temperature on the gas response of porous ZnO microspheres to 50 ppm ethanol gas. (b) Selectivity of porous ZnO microspheres to different testing gases. (c) Selectivity of ZnO microspheres versus testing gases concentration. (d) Response and recovery curves of porous ZnO microspheres upon exposure to ethanol gas.

of the sensors based on porous ZnO microspheres could be selected as 280°C. Figure 8(b) shows the responses of the as-prepared sensors to the various organic vapors, such as formaldehyde, ammonia, ethanol, and acetone with the concentration of 100 ppm at an operating temperature of 280°C. It is clearly found that the response of sensor to ethanol gas was highest among the test gases. Consequently, the sensor based on porous ZnO microspheres showed good selectivity toward ethanol compared to the other gases at the operating temperature of 280°C. The sensing properties of porous ZnO microspheres sensors to 5, 10, 50, and 100 ppm of formaldehyde, ammonia, ethanol, and acetone are measured at 280°C, as shown in Figure 8(c). The sensor has a larger value of response to ethanol but worse response to formaldehyde, ammonia, and acetone under the same concentration. These findings confirm the superior selectivity of porous ZnO microspheres sensors to ethanol. Figure 8(d) displays response and recovery curves of the ZnO sensors to ethanol gas with different concentrations (5 to 500 ppm) at an operating temperature of 280°C. According to Figure 8(d), it can be observed that the sensor exhibits fast response and recovery times, and the sensitivity of porous ZnO to ethanol gases increased with the increasing of ethanol concentration. The response time and recovery time of the as-fabricated porous ZnO microspheres sensor for 5 ppm ethanol were 4 s and 2 s, respectively (inset of Figure 8(d)).

The gas-sensing mechanism of 3D porous ZnO microspheres can be explained by the surface charge model [32]. When exposed in different type of gases, resistance of semiconductor oxide materials alters. When the ZnO sensor is exposed in air, oxygen molecules in the atmosphere are absorbed on the surface of ZnO nanosheets by capturing free electrons from the conduction band, generating oxygen ions, such as O_2^-, O^-, and O^{2-} [1, 33], leading to the electron concentration of the conduction band decreasing and the resistance of ZnO sensor increasing. The surface reactions can be described as follows:

$$O_2\,(\text{gas}) + e^- \longrightarrow O_2^-\,(\text{absorbed}) \qquad (8)$$

$$O_2\,(\text{gas}) + 2e^- \longrightarrow 2O^-\,(\text{absorbed}) \quad (9)$$

$$O^-\,(\text{absorbed}) + e^- \longrightarrow O^{2-}\,(\text{absorbed}) \quad (10)$$

When ZnO is exposed to the ethanol gas, the ethanol molecules will react with the adsorbed oxygen ions on the surface and release the electrons back to the conduction band. This results in the electron concentration increasing and as a consequence the resistance of the materials decreases. The chemical reactions can be written as follows:

$$C_2H_5OH + O^- \longrightarrow C_2H_4O + H_2O + e^- \quad (11)$$

$$C_2H_5OH + O^{2-} \longrightarrow C_2H_4O + H_2O + 2e^- \quad (12)$$

$$2C_2H_5OH + O_2{}^- \longrightarrow 2C_2H_4O + 2H_2O + e^- \quad (13)$$

When increasing the concentration of ethanol, more and more electrons were released back to the conduction band, leading to the resistance of sensors decreasing. That is why the sensitivity of porous ZnO to ethanol gases increased with the increasing of ethanol concentration.

Moreover, the reasons for the superior gas-sensing properties of porous ZnO microspheres were possibly attributed to the abundant pores increasing the specific surface areas. It was well known that large specific surface areas provided more active sites and promoted gas diffusion. Thus, the porous ZnO microspheres were promising candidates for gas-sensing applications, especially for the detection of ethanol.

4. Conclusions

In summary, the porous ZnO microspheres have been successfully synthesized by calcining the ZHC precursor microsphere, which were the reaction products of a hydrothermal reaction by zinc nitrate hexahydrate and urea in the presence of trisodium citrate. The porous ZnO microspheres are assembled by numerous porous nanosheets. The approach provided a simple, effective, low-cost, and environment friendly method to largely synthesize the porous ZnO microspheres. Furthermore, the formation mechanism of the porous ZnO microspheres was speculated by the experimental results and analysis. The gas-sensing properties test indicated that the ZnO gas sensors exhibit excellent sensing performances to ethanol, owing to their large specific surface area and outstanding gas-sensing properties. The porous ZnO microspheres were promising candidates for the applications of ethanol sensitive material.

Conflict of Interests

The authors declare that there is no conflict of interests regarding the publication of this paper.

Acknowledgments

This work is supported by the National Natural Science Foundation of China (nos. 51372103 and 51202092), the special grade of the financial support from China Postdoctoral Science Foundation (2014T70485), and the China Postdoctoral Science Foundation (2013M531285).

References

[1] L. L. Wang, H. M. Dou, F. Li, J. N. Deng, Z. Lou, and T. Zhang, "Controllable and enhanced HCHO sensing performances of different-shelled ZnO hollow microspheres," *Sensors and Actuators B: Chemical*, vol. 183, pp. 467–473, 2013.

[2] C.-T. Lee and T.-J. Wu, "Light distribution and light extraction improvement mechanisms of remote GaN-based white light-emitting-diodes using ZnO nanorod array," *Journal of Luminescence*, vol. 137, pp. 143–147, 2013.

[3] C. T. Pan, Y. C. Chen, C. C. Hsieh et al., "Ultrasonic sensing device with ZnO piezoelectric nanorods by selectively electrospraying method," *Sensors and Actuators A: Physical*, vol. 216, pp. 318–327, 2014.

[4] N. Uekawa, T. Saito, T. Kojima, and K. Kakegawa, "Control of orientation and electrical conductivity of doped ZnO films using a layered double hydroxide nanoparticle precursor and spark plasma sintering process," *Scripta Materialia*, vol. 69, no. 2, pp. 131–134, 2013.

[5] J. R. Huang, H. B. Ren, P. P. Sun, C. P. Gu, Y. F. Sun, and J. H. Liu, "Facile synthesis of porous ZnO nanowires consisting of ordered nanocrystallites and their enhanced gas-sensing property," *Sensors and Actuators B: Chemical*, vol. 188, pp. 249–256, 2013.

[6] X. H. Zhao, F. J. Lou, M. Li, X. D. Lou, Z. Z. Li, and J. G. Zhou, "Sol-gel-based hydrothermal method for the synthesis of 3D flower-like ZnO microstructures composed of nanosheets for photocatalytic applications," *Ceramics International*, vol. 40, no. 4, pp. 5507–5514, 2014.

[7] S. J. Pearton and F. Ren, "Advances in ZnO-based materials for light emitting diodes," *Current Opinion in Chemical Engineering*, vol. 3, pp. 51–55, 2014.

[8] D. Y. Jiang, J. Y. Zhang, Y. M. Lu et al., "Ultraviolet Schottky detector based on epitaxial ZnO thin film," *Solid-State Electronics*, vol. 52, no. 5, pp. 679–682, 2008.

[9] S. S. Ma, R. Li, C. P. Lv, W. Xu, and X. L. Gou, "Facile synthesis of ZnO nanorod arrays and hierarchical nanostructures for photocatalysis and gas sensor applications," *Journal of Hazardous Materials*, vol. 192, no. 2, pp. 730–740, 2011.

[10] B.-H. Lee and S.-M. Kang, "Properties of ZnO varistor blocks under multiple lightning impulse voltages," *Current Applied Physics*, vol. 6, no. 5, pp. 844–851, 2006.

[11] M. Raja, N. Muthukumarasamy, D. Velauthapillai, R. Balasundaraprabhu, S. Agilan, and T. S. Senthil, "Studies on bundle like ZnO nanorods for solar cell applications," *Solar Energy*, vol. 106, pp. 129–135, 2014.

[12] R. Murugan, T. Woods, P. Fleming, D. Sullivan, S. Ramakrishna, and P. R. Babu, "Synthesis and photocatalytic application of ZnO nanoarrows," *Materials Letters*, vol. 128, pp. 404–407, 2014.

[13] Q. Hou, L. Q. Zhu, H. N. Chen, H. C. Liu, and W. P. Li, "Growth of flower-like porous ZnO nanosheets by electrodeposition with $Zn_5(OH)_8(NO_3)_2 \bullet 2H_2O$ as precursor," *Electrochimica Acta*, vol. 78, pp. 55–64, 2012.

[14] C.-F. Li, C.-Y. Hsu, and Y.-Y. Li, "NH_3 sensing properties of ZnO thin films prepared via sol-gel method," *Journal of Alloys and Compounds*, vol. 606, pp. 27–31, 2014.

[15] G. C. Qi, S. Z. Zhao, and Z. H. Yuan, "From function-guided assembly of a lotus leaf-like ZnO nanostructure to a formaldehyde gas-sensing application," *Sensors and Actuators B: Chemical*, vol. 184, pp. 143–149, 2013.

[16] Y. Zeng, L. Qiao, Y. F. Bing et al., "Development of microstructure CO sensor based on hierarchically porous ZnO nanosheet thin films," *Sensors and Actuators B: Chemical*, vol. 173, pp. 897–902, 2012.

[17] A. Mortezaali and R. Moradi, "The correlation between the substrate temperature and morphological ZnO nanostructures for H_2S gas sensors," *Sensors and Actuators A: Physical*, vol. 206, pp. 30–34, 2014.

[18] S. H. Wei, S. M. Wang, Y. Zhang, and M. H. Zhou, "Different morphologies of ZnO and their ethanol sensing property," *Sensors and Actuators B: Chemical*, vol. 192, pp. 480–487, 2014.

[19] C.-J. Chang, C.-Y. Lin, J.-K. Chen, and M.-H. Hsu, "Ce-doped ZnO nanorods based low operation temperature NO_2 gas sensors," *Ceramics International*, vol. 40, no. 7, pp. 10867–10875, 2014.

[20] M. S. Samuel, J. Koshy, A. Chandran, and K. C. George, "Electrical charge transport and dielectric response in ZnO nanotubes," *Current Applied Physics*, vol. 11, no. 4, pp. 1094–1099, 2011.

[21] M. Raja, N. Muthukumarasamy, D. Velauthapillai, and R. Balasundaraprabhu, "Influence of copper on the morphology and properties of one dimensional ZnO nanorod structures," *Superlattices and Microstructures*, vol. 72, pp. 102–110, 2014.

[22] G. Meng, X. D. Fang, W. W. Dong et al., "One step synthesis of vertically aligned ZnO nanowire arrays with tunable length," *Applied Surface Science*, vol. 256, no. 22, pp. 6543–6549, 2010.

[23] R. Zhang, M. Hummelgård, and H. Olin, "A facile one-step method for synthesising a parallelogram-shaped single-crystalline ZnO nanosheet," *Materials Science and Engineering B*, vol. 184, no. 1, pp. 1–6, 2014.

[24] J. Karamdel, C. F. Dee, and B. Y. Majlis, "Characterization and aging effect study of nitrogen-doped ZnO nanofilm," *Applied Surface Science*, vol. 256, no. 21, pp. 6164–6167, 2010.

[25] C. P. Gu, J. R. Huang, Y. J. Wu, M. H. Zhai, Y. F. Sun, and J. H. Liu, "Preparation of porous flower-like ZnO nanostructures and their gas-sensing property," *Journal of Alloys and Compounds*, vol. 509, no. 13, pp. 4499–4504, 2011.

[26] B. X. Li and Y. F. Wang, "Hierarchically assembled porous ZnO microstructures and applications in a gas sensor," *Superlattices and Microstructures*, vol. 49, no. 4, pp. 433–440, 2011.

[27] F. B. Gu, D. You, Z. H. Wang, D. M. Han, and G. S. Guo, "Improvement of gas-sensing property by defect engineering in microwave-assisted synthesized 3D ZnO nanostructures," *Sensors and Actuators B: Chemical*, vol. 204, pp. 342–350, 2014.

[28] C. Li, G. J. Fang, W. J. Guan, and X. Z. Zhao, "Multipod ZnO 3D microstructures," *Materials Letters*, vol. 61, no. 14-15, pp. 3310–3313, 2007.

[29] X. L. Cai, F. X. Wang, D. W. Yan, Z. M. Zhu, and X. F. Gu, "Luminescence characteristics and growth mechanism of awl-like ZnO Nanostructures fabricated on Ni-coated silicon substrate via chemical vapor deposition method," *Ceramics International*, vol. 40, no. 8, pp. 12293–12298, 2014.

[30] M. Shamsipur, S. M. Pourmortazavi, S. S. Hajimirsadeghi, M. M. Zahedi, and M. Rahimi-Nasrabadi, "Facile synthesis of zinc carbonate and zinc oxide nanoparticles via direct carbonation and thermal decomposition," *Ceramics International*, vol. 39, no. 1, pp. 819–827, 2014.

[31] C. L. Shao, L. Tu, A. Yu, B. Li, and X. F. Zhou, "From $Zn_4(CO_3)(OH)_6{\cdot}H_2O$ curling nanopetals to ZnO stretching porous nanosheets: growth mechanism and gas sensing property," *Thin Solid Films*, vol. 525, pp. 148–153, 2012.

[32] W. W. Guo, T. N. Liu, J. X. Wang et al., "Hierarchical ZnO porous microspheres and their gas-sensing properties," *Ceramics International*, vol. 39, no. 5, pp. 5919–5924, 2013.

[33] J. S. Cui, J. B. Sun, X. Liu, J. W. Li, X. Z. Ma, and T. T. Chen, "Fabrication of hierarchical flower-like porous ZnO nanostructures from layered $ZnC_2O_4{\cdot}3Zn(OH)_2$ and gas sensing properties," *Applied Surface Science*, vol. 308, pp. 17–23, 2014.